Electronic Supplementary Material (ESI) for Polymer Chemistry.

Supporting Information for Polymer Chemistry manuscript:

Synthesis and characterization of poly(amino acid methacrylate)-stabilized diblock copolymer nano-objects

Vincent Ladmiral,* Alexandre Charlot, Mona Semsarilar, Steven P. Armes*

Note regarding RAFT agent efficiency

Differences between the mean DP calculated by ^{1}H NMR end-group analysis and the DP calculated using the following equation DP = (n_{M0}/n_{RAFT0}) x conversion, (where n_{M0} and n_{RAFT0} are, respectively, the molar quantities of monomer and RAFT agent introduced in the reaction at t = 0) were observed.

^{1}H NMR end-group analysis of RAFT polymers is based on the assumption that every polymer chain possesses the Z-group of the RAFT agent at its ω-end. Several reactions can occur in the course of the polymerization, or during purification/work-up that might undermine this assumption: (1) premature termination between polymer radicals or via their reaction with other radicals; (2) hydrolysis of the trithiocarbonate group during either synthesis or work-up (e.g. dialysis); (3) lower than expected participation of the RAFT agent in the polymerization.; (4) error in the mass of RAFT agent and/or monomer actually used for the polymerization; (5) impurities in the RAFT agent. In our calculations, chain transfer does not have any impact since this side reaction does not reduce the number of RAFT end-groups. Nonetheless, it is very difficult to identify the cause of the difference between the DP calculated from ^{1}H NMR end-group analysis and the theoretically expected DP. We have chosen to interpret this discrepancy in terms of RAFT agent (in)efficiency.

Figure S1. NMR signal assignment for GSHMA

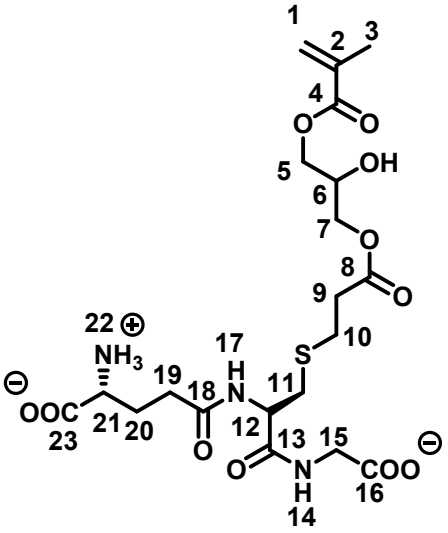

^{1}H NMR (400.13 MHz, DMSO-d_6, 298K): δ 1.95 (s, $3H_3$), 2.15 (dd, $2H_{19}$), 2.50-2.54 (dt, $2H_{20}$), 2.74-2.89 (m, $2H_9$, $2H_{10}$, $2H_{11}$), 3.06-3.11(dd, $1H_{12}$), 3.34 (t, 1H, OH), 3.71-3.80 (m, 4H, $1H_6$, $2H_{15}$, $1H_{21}$), 4.20-4.25 (m, 4H, $2H_5$, $2H_7$), 5.77 (d, $1H_1$'), 6.18 (d, $1H_1$), 8.19 (t, $1H_{14}$), 8.52 (d, $3H_{22}$).

^{13}C NMR (400.13 MHz, DMSO-d_6, 298K): δ 17.5 (C_3), 26.3 (C_{20}), 26.7 (C_{10}), 31.5 (C_{19}), 33.0 (C_{11}), 34.2 (C_9), 43.5 (C_{15}), 54.2 (C_6), 62.1 (C_{21}), 65.3 (2C, C_5, C_7), 66.9 (C_{12}), 127.3 (C_1), 135.6 (C_2), 169.3, 171.8, 174.0, 174.8, 176.1, 177.1 (6C, C_4, C_8, C_{13}, C_{16}, C_{18}, C_{23}).

Figure S2. Acid titration of glutathione methacrylate (GSHMA)

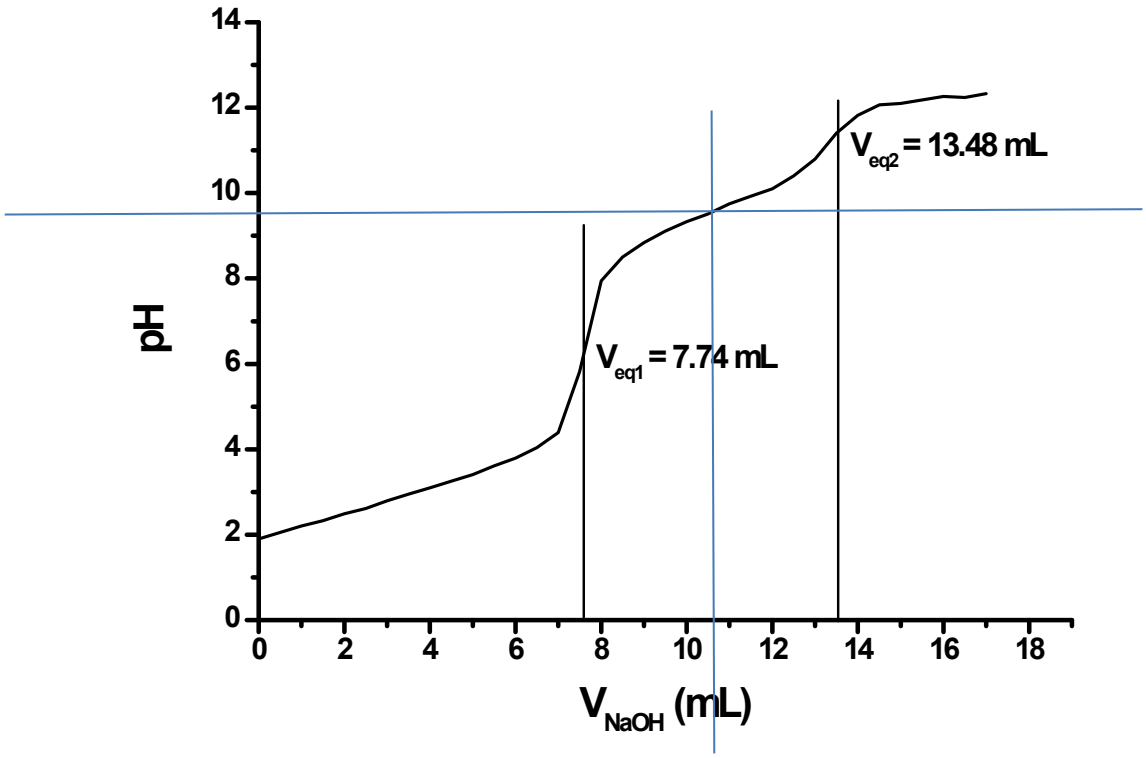

V_0 = 1mL of GSHMA solution was diluted to 5 mL with DI water and titrated with an aqueous 75 mM NaOH solution. $[GSHMA]_0 = ((V_{eq2}-V_{eq1})^* c_{NaOH})/ V_0 = 0.438$ M.

Figure S3. DMF GPC chromatograms obtained for $PCysMA_{31}$ and $PGSHMA_{24}$

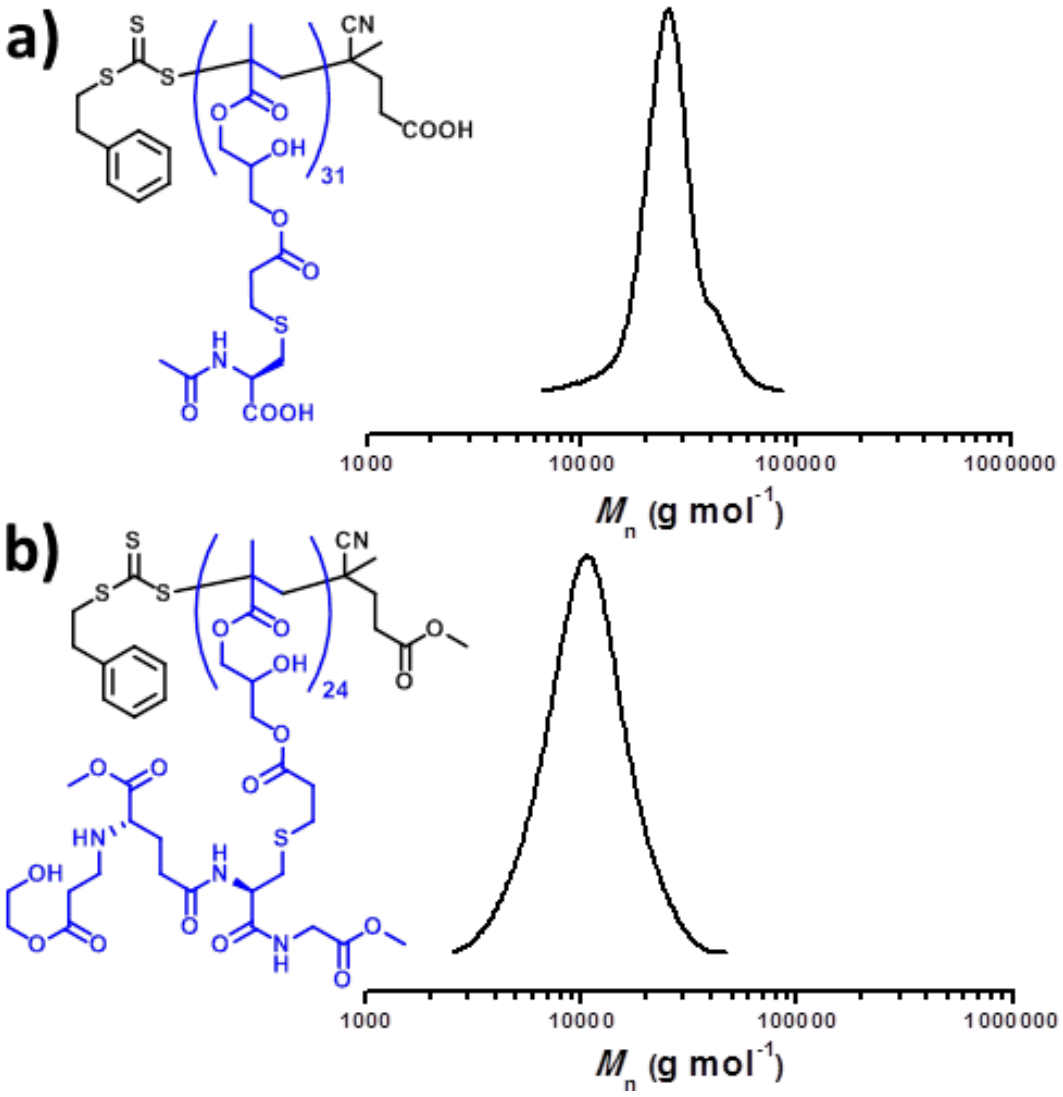

DMF gel permeation chromatograms recorded for: (a) $PCysMA_{31}$, 94 % conversion, $M_{n\ (NMR)}$ = 10,700 g mol^{-1}, M_w/M_n = 1.11; (b) $PGSHMA_{24}$, 98 % conversion, $M_{n\ (NMR)}$ = 12,800 g mol^{-1}, M_w/M_n = 1.20. $PCysMA_{31}$ and $PGSHMA_{24}$ were derivatized (acetylation using acetic anhydride for $PCysMA_{31}$ and both Michael addition with 2-hydroxyethyl acrylate and methylation with trimethylsilyl diazomethane in the case of $PGSHMA_{24}$) prior to GPC analysis.

Figure S4. RAFT solution polymerization of cysteine methacrylate (CysMA)

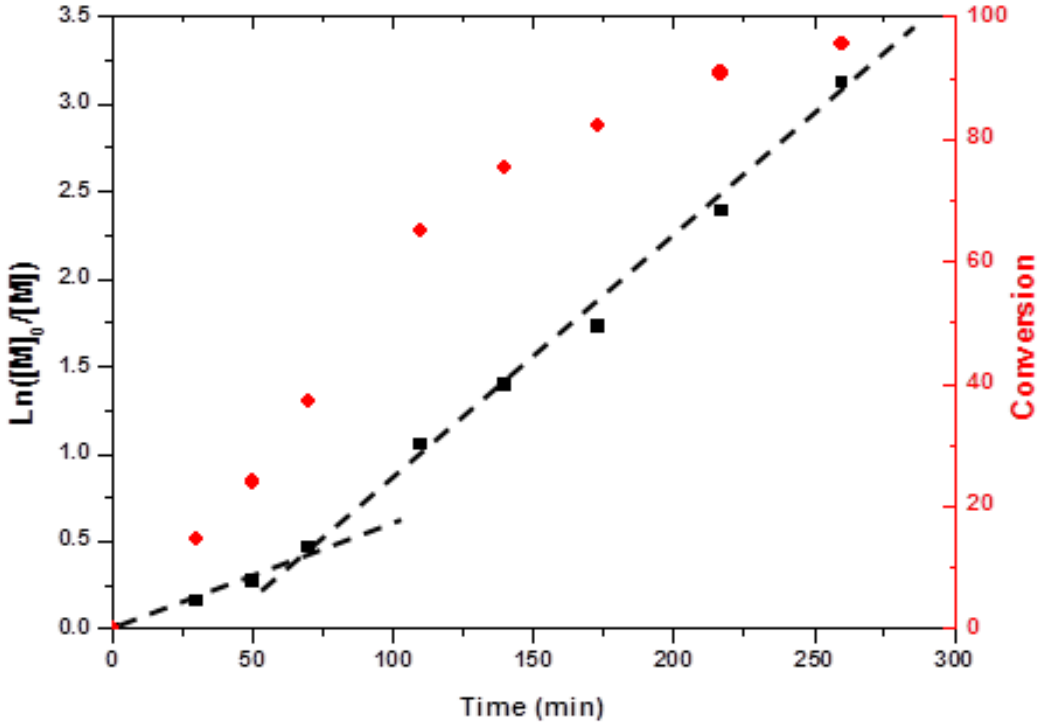

First-order kinetic plot and evolution of conversion vs time for the RAFT polymerization of CysMA in an 83:17 w/w water/dioxane mixture at 70 °C. Reaction conditions: [CysMA] : [PETTC] : [ACVA] = 50 : 1 : 0.2, [CysMA] = 9 wt %.

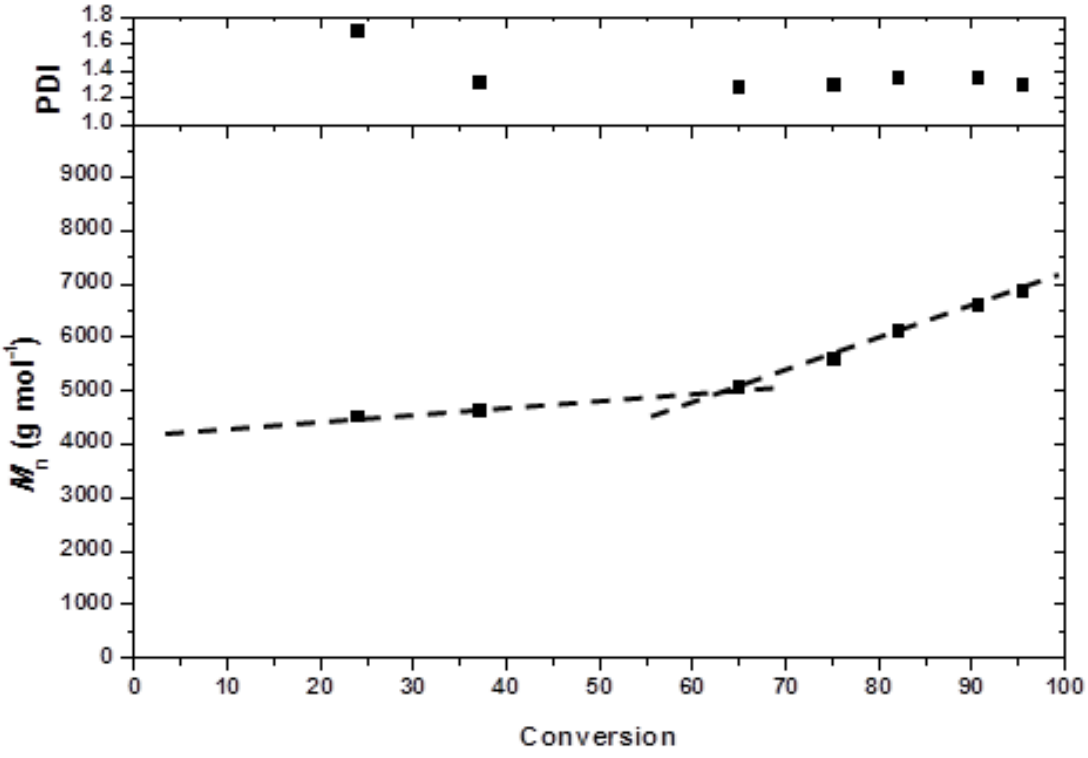

Evolution of M_n and polydispersity vs conversion for the RAFT polymerization of CysMA in an 83:17 w/w water/dioxane mixture at 70 °C. Reaction conditions: [CysMA] : [PETTC] : [ACVA] = 50 : 1 : 0.2, [CysMA] = 9 wt %.

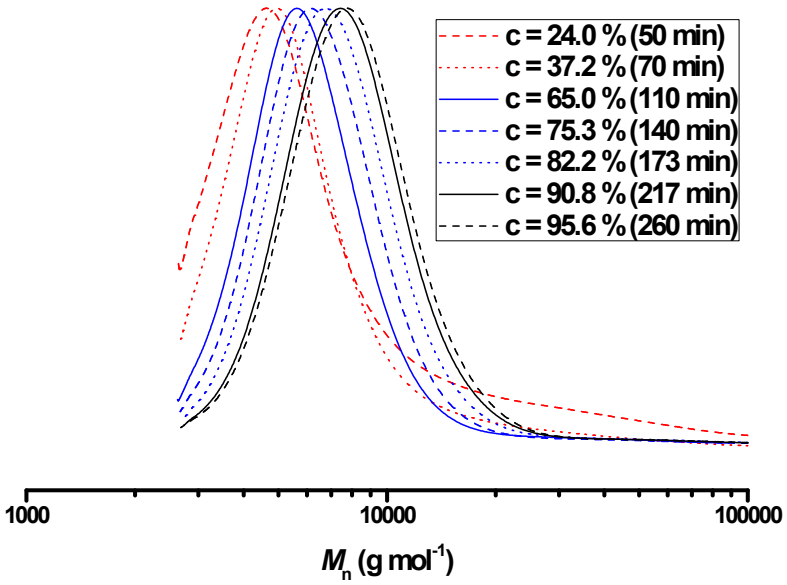

Aqueous GPC chromatograms obtained for samples taken at different times during the RAFT solution polymerization of CysMA in water/dioxane mixture.

Figure S5. Phase diagram and representative TEM images obtained for the RAFT aqueous dispersion polymerization of HPMA using a $PGSHMA_{24}$ macro-CTA

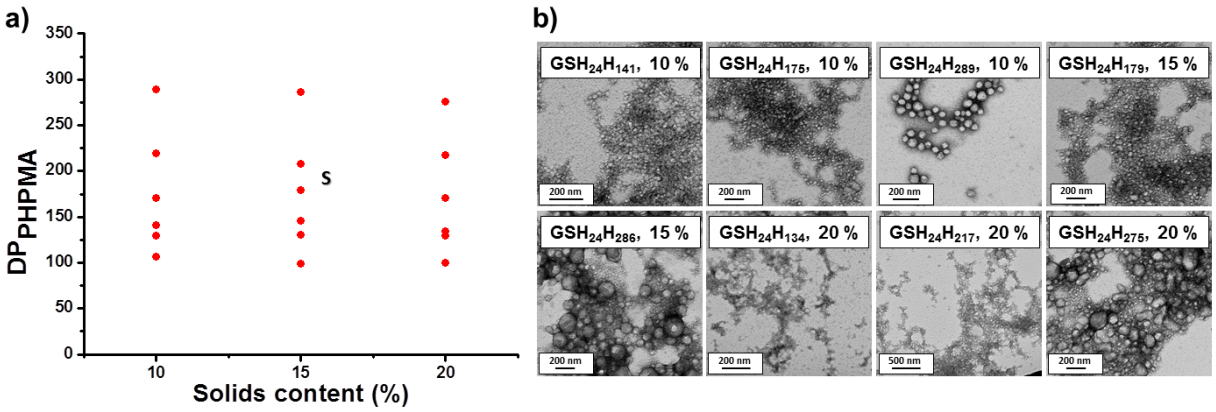

(a) Phase diagram constructed for $PGSHMA_{24}$–$PHPMA_x$ diblock copolymer nano-objects prepared by RAFT aqueous dispersion polymerization of HPMA using a $PGSHMA_{24}$ macro-CTA at 70˚C. The target PHPMA DP and the total solids content were systematically varied and the *post mortem* copolymer morphologies obtained at > 98 % HPMA conversion were determined by TEM. N.B. S denotes spheres.

(b) Representative TEM images obtained for $PGSHMA_{24}$–$PHPMA_x$ (denoted GSH_{24}–H_x for brevity) diblock copolymer nano-objects prepared by RAFT aqueous dispersion polymerization of HPMA at 70 °C. The target block composition and copolymer solids content % are indicated on each image.

Figure S6. TEM images obtained for diblock copolymer nano-objects formed in the presence of NaCl

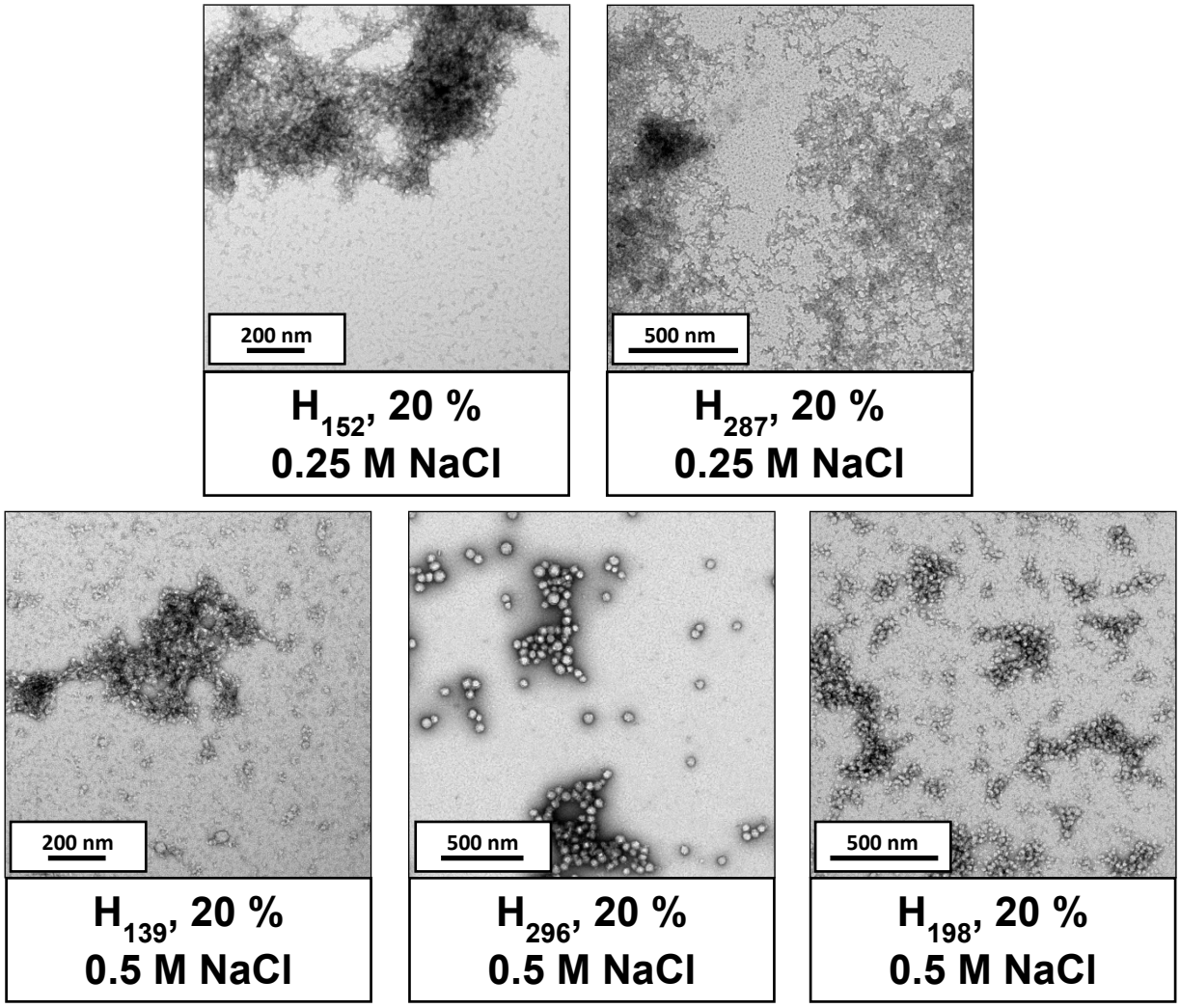

Representative TEM images obtained for $PGSHMA_{24}$–$PHPMA_x$ diblock copolymer nano-objects prepared by RAFT aqueous dispersion polymerization of HPMA at 70 °C in the presence of NaCl. The targeted DP for the PHPMA block (herein denoted by 'H' for brevity) and the copolymer solids content % is indicated on each image.

Figure S7. TEM images obtained for diblock copolymer nano-objects prepared using relatively short PGSHMA macro-CTAs

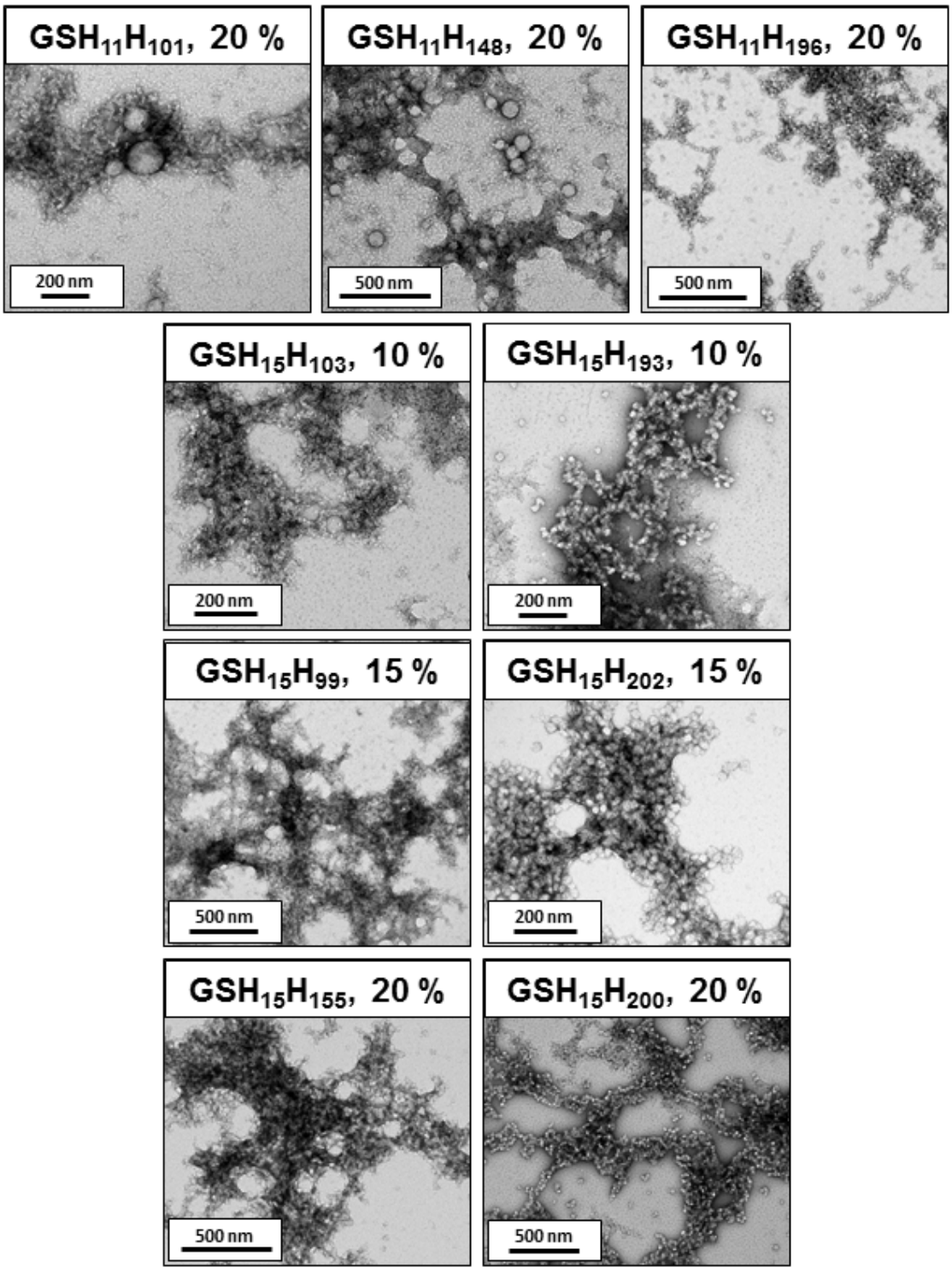

Representative TEM images obtained for $PGSHMA_{11}$–$PHPMA_x$ and $PGSHMA_{15}$–$PHPMA_x$ diblock copolymer nano-objects prepared by RAFT aqueous dispersion polymerization of HPMA at 70 °C. The targeted DP for the PHPMA block (herein denoted by 'H' for brevity) and the copolymer solids content % is indicated on each image.

Figure S8. DMF GPC chromatogram obtained for $PGMA_{55}$ macro-CTA

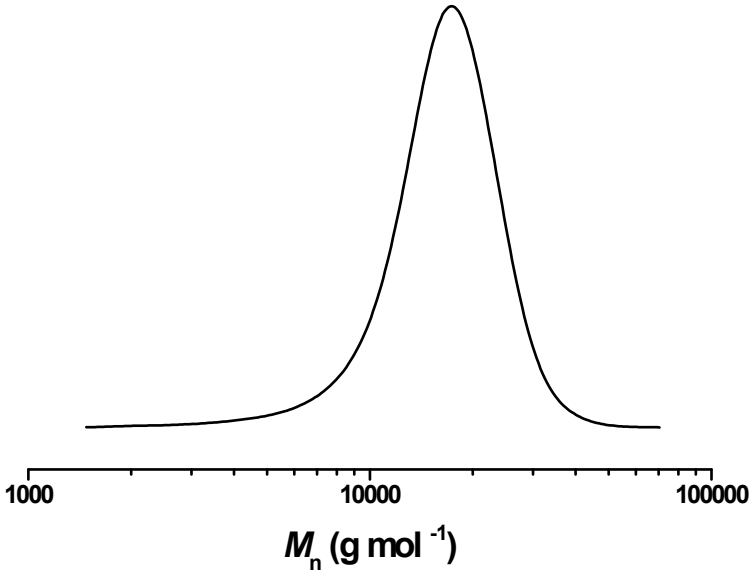

DMF GPC chromatogram obtained for $PGMA_{55}$:

M_n = 15,100 g mol^{-1}, M_w = 19,600 g mol^{-1}, M_w / M_n = 1.15

Figure S9. Temperature dependence of the storage and loss moduli observed for a 20 % w/w PGSHMA$_{24}$ + PGMA$_{55}$)-PHPMA$_{178}$ diblock copolymer worm gel dispersion

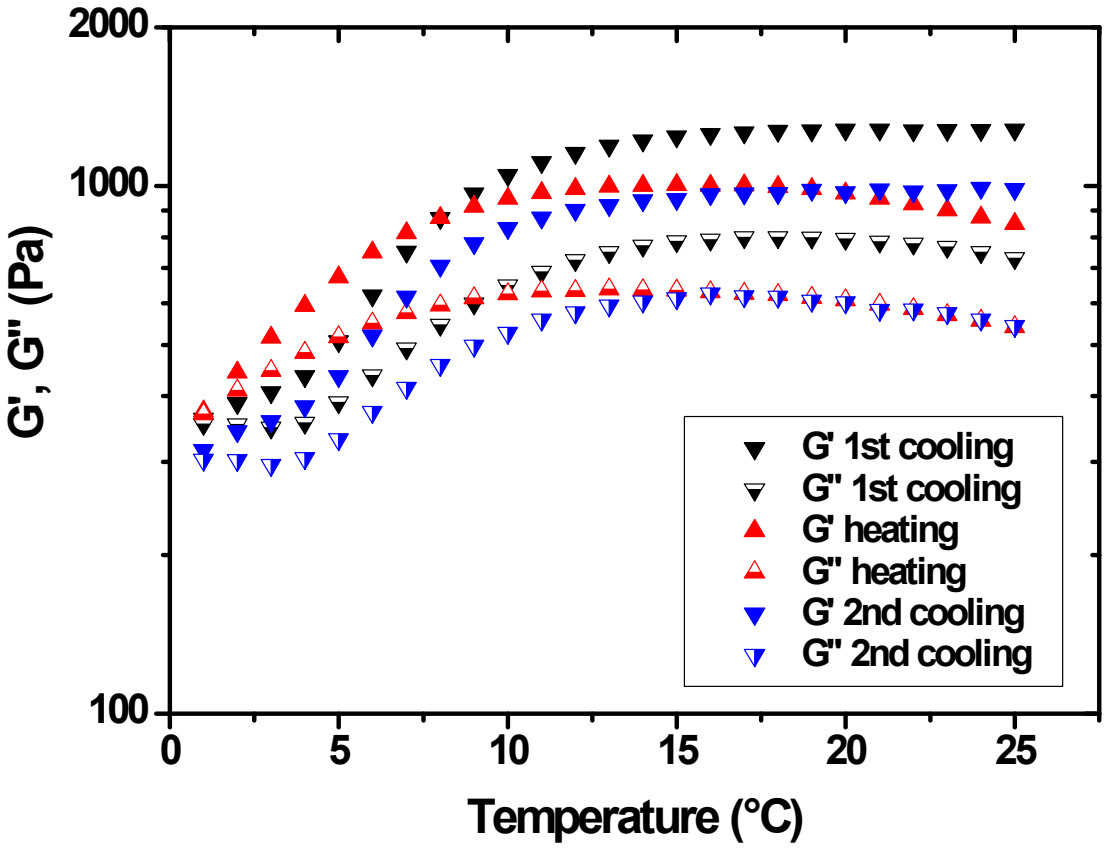

Variation of storage modulus (G') and loss modulus (G'') for a 20% w/w (1:9 PGSHMA$_{24}$ + PGMA$_{55}$)-PHPMA$_{178}$ diblock copolymer worm gel dispersion during the following temperature cycling: (i) cooling from 25 to 1 °C (G' = inverted black triangles, G'' = inverted black and white triangles); (ii) subsequent warming from 1 to 25 °C in 1 °C increments (G' = red triangles, G'' = red and white triangles) and (iii) cooling from 25 to 1 °C in 1 °C increments (G' = inverted blue triangles, G'' = inverted blue and white triangles).

Notes: The cross-over temperature appeared to be slightly below 1 °C in this case.

Hysteresis is observed between the first cooling and heating cycles. This was much less marked between the heating and the second cooling cycles.

Figure S10. Temperature-dependent DLS studies of diblock copolymer worm dispersions

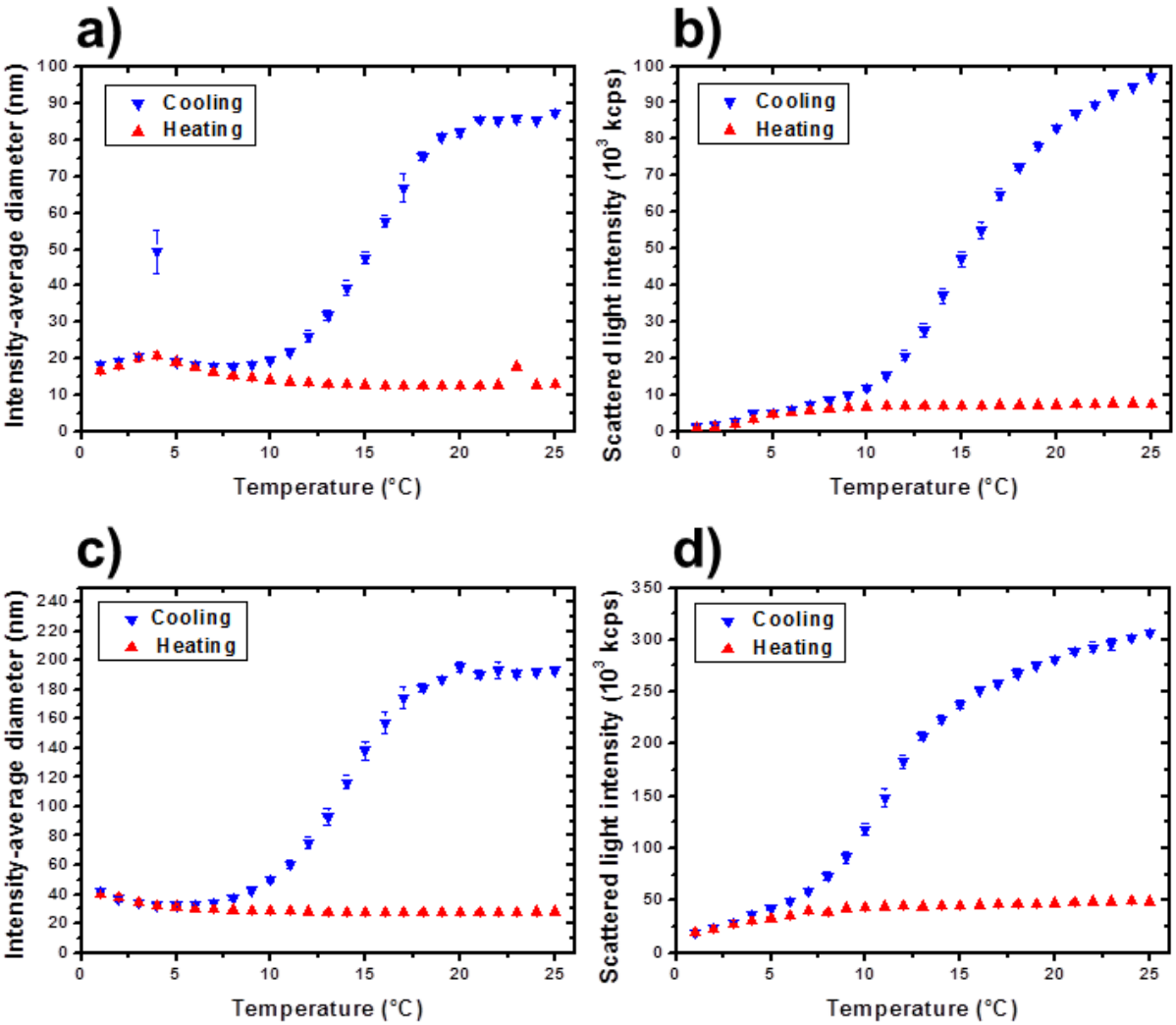

Temperature-dependent DLS studies, showing the variation in intensity-average diameter and scattered light intensity respectively, for: (a, b) a (1:9 $PCysMA_{31}$ + $PGMA_{55}$)-$PHPMA_{166}$ dispersion of diblock copolymer worms diluted to 1% w/w; (c, d) a (1:9 $PGSHMA_{24}$ + $PGMA_{55}$)-$PHPMA_{178}$ dispersion of diblock copolymer worms diluted to 1.0% w/w.

In the case of (1:9 $PCysMA_{31}$ + $PGMA_{55}$)-$PHPMA_{166}$ (see Figures S10a and S10b), the apparent sphere-equivalent hydrodynamic diameter decreases from around 90 nm at 25°C to 20 nm at 1°C, with a concomitant reduction in the scattered light intensity. These measurements are consistent with visual observations and rheological data and confirm that degelation occurs via a worm-to-sphere transition. However, on warming the cold 1% w/w copolymer dispersion to ambient temperature, the sphere-to-worm transition is *not* observed, even on standing for relatively long time scales (weeks). This is because of the reduced probability of efficient 1D fusion of spheres at this relatively low copolymer concentration.[76b]

The DLS data (see Figures S11c and S11d) are very similar to those obtained for a dilute dispersion of (1:9 $PCysMA_{31}$ + $PGMA_{55}$)-$PHPMA_{166}$. Thus cooling a 1% w/w dispersion of (1:9 $PGSHMA_{24}$ + $PGMA_{55}$)-$PHPMA_{178}$ diblock copolymer nano-objects results in a near-monotonic reduction in particle size and scattered light intensity. Polydisperse worms with a sphere-equivalent diameter of 180 nm were observed at 25°C, while near-monodisperse spheres of 40 nm were obtained below 10°C. No sphere-to-worm transition occurred on returning to 25°C, confirming that the (ir)reversibility of this thermal transition has a strong concentration dependence.

Figure S11. Variation of zeta potential and intensity-average diameter with pH for spheres, worms and vesicles.

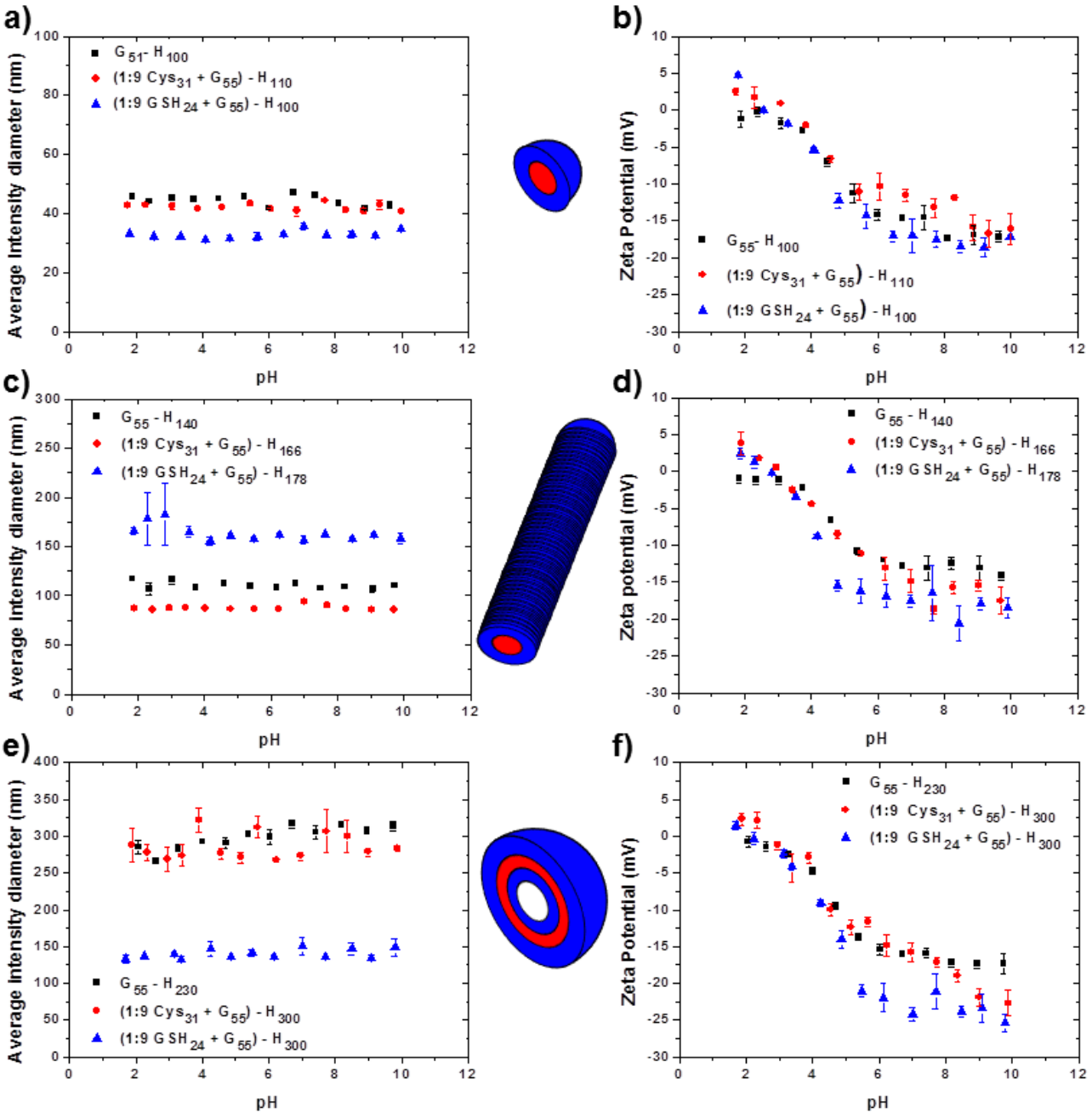

Variation of zeta potential and intensity-average diameter with pH for spheres, worms and vesicles. (a) Intensity-average diameter vs. pH for $PGMA_{55}$-$PHPMA_{100}$ spheres (black squares), (1:9 $PCysMA_{31}$ + $PGMA_{55}$)-$PHPMA_{110}$ (red circles), and (1:9 $PGSHMA_{24}$ + 0.9$PGMA_{55}$)-$PHPMA_{100}$ (blue triangles). (b) Zeta potential vs. pH for the same diblock copolymer dispersions. (c) Intensity-average diameter vs pH for $PGMA_{55}$-$PHPMA_{140}$ worms (black squares), (1:9 $PCysMA_{31}$ + $PGMA_{55}$)-$PHPMA_{166}$ (red circles), and (1:9 $PGSHMA_{24}$ + $PGMA_{55}$)-$PHPMA_{178}$ (blue triangles). (d) Zeta potential vs. pH for the same diblock copolymer dispersions. (e) Intensity diameter vs pH for $PGMA_{55}$-$PHPMA_{230}$ vesicles (black squares), (1:9 $PCysMA_{31}$ + $PGMA_{55}$)-$PHPMA_{300}$ (red circles), and (1:9 $PGSHMA_{24}$ + $PGMA_{55}$)-$PHPMA_{300}$ (blue triangles). (f) Zeta potential vs. pH for the same diblock copolymer dispersions.